

Technical Note

# Characterizing the Development of Photovoltaic Power Stations and Their Impacts on Vegetation Conditions from Landsat Time Series during 1990–2022

Su Ma <sup>1</sup>, Junhui Liu <sup>1,\*</sup>, Ping Zhang <sup>2,†</sup>, Xingyue Tu <sup>1</sup>, Jianan Zhou <sup>1</sup>, Yang Liu <sup>1</sup> and Yingjuan Zheng <sup>1</sup>

<sup>1</sup> Chinese Research Academy of Environmental Sciences, Beijing 100012, China; ma.su@craes.org.cn (S.M.); tu.xingyue@craes.org.cn (X.T.); jnzhou\_leona@163.com (J.Z.); liu.yang@craes.org.cn (Y.L.); zhengyj@craes.org.cn (Y.Z.)

<sup>2</sup> National Geomatics Center of China, Beijing 100830, China; zhangping@ngcc.cn

\* Correspondence: liujh@craes.org.cn

† These authors contributed equally to this work.

**Abstract:** To achieve carbon peaking and carbon neutrality in China, photovoltaic (PV) power generation has become increasingly important for promoting a low-carbon transition. The central and western desert areas of China have been identified as major areas for the construction of large PV bases. Remote sensing technology has been used to map the spatial distribution and development status of PV power stations quickly and accurately in ecologically fragile areas, as well as assess the ecological and environmental impact of their construction. However, current remote sensing monitoring of PV power stations focuses mainly on mapping and time series analysis to measure their development process and assess the environmental conditions on a large scale over a long period of time. Therefore, we constructed a random forest model based on image spectral and texture features and mapped 2022 PV power stations in the junction area of Hobq Desert, Ulan Buh Desert, Tengger Desert, and Mu Us Sands in China. Following that, we identified the construction time of the PV power stations by identifying the turning points of the normalized construction land index (NDBI) time series from 1990–2022 using the LandTrendr method. To assess the ecological impact of PV power stations, we used the NDVI to measure the change in vegetation condition before and after the construction of PV power stations and constructed NDVI changes for PV power stations constructed in different years. The results showed that this mapping method achieved an overall classification accuracy of 96.65% and a Kappa coefficient of 0.92. The root mean square error (RMSE) for construction year identification was less than 0.5, and the number of new PV power stations increased significantly after 2010, reaching a total area of 14.52 km<sup>2</sup> by 2016, which is consistent with the trend driven by national and regional development plans. Furthermore, the study found that the vegetation cover level could be restored to the average level before construction within 5–6 years and continued to increase after that. These findings may help government policymakers and practitioners make decisions on PV power station planning and ecological environment protection, thus contributing promptly to the achievement of China's dual carbon goals.

**Keywords:** photovoltaic power stations; random forest; time series analysis; ecological and environmental effects; Landsat



**Citation:** Ma, S.; Liu, J.; Zhang, P.; Tu, X.; Zhou, J.; Liu, Y.; Zheng, Y. Characterizing the Development of Photovoltaic Power Stations and Their Impacts on Vegetation Conditions from Landsat Time Series during 1990–2022. *Remote Sens.* **2023**, *15*, 3101. <https://doi.org/10.3390/rs15123101>

Academic Editor: Dino Ienco

Received: 27 April 2023

Revised: 30 May 2023

Accepted: 5 June 2023

Published: 14 June 2023



**Copyright:** © 2023 by the authors. Licensee MDPI, Basel, Switzerland. This article is an open access article distributed under the terms and conditions of the Creative Commons Attribution (CC BY) license (<https://creativecommons.org/licenses/by/4.0/>).

## 1. Introduction

With the ongoing energy crisis and the increasing threat of global warming, many countries are shifting towards clean energy sources to combat the issue [1,2]. Recently, China officially proposed that CO<sub>2</sub> emissions strive to peak in 2030 and achieve carbon neutrality by 2060. Since solar energy has naturally high availability and relatively low negative impacts on the environment [3,4], PV power generation has become an important way for China to promote energy transformation, protect the ecological environment,

mitigate climate change, and achieve the goals of carbon peaking and carbon neutrality [5,6]. China's PV power station construction has ranked first in the world for many years. The new and cumulatively installed PV capacity of China will account for more than one-third of the total installed global wind power PV capacity by 2022 [7]. Desert areas rich in solar energy resources, especially Hobq Desert, Ulan Buh Desert, Tengger Desert, and Mu Us Sands [8], are preferred to locate PV construction bases, accounting for more than 60% of the total installed capacity of China. However, these areas also happen to be ecologically fragile. For such areas, understanding the ecological impact of the rapid and massive construction of PV power stations is very important for optimizing the layout of PV power stations and protecting the regional ecology.

Remote sensing technology has the advantages of timely and efficient large-scale synchronous monitoring [9], and efforts have been made to map PV power stations predominantly through visual interpretation, machine learning, and deep learning over the last few years [10–14]. Visual interpretation is an accurate and easy-to-implement approach for identifying densely located PV power stations. However, it is time-consuming and laborious for large-scale mapping. Deep learning methods are suitable for large-scale and automatic mapping. Their data acquisition and computation are expensive. Random forest (RF) can be used to process high-dimensional data quickly and accurately for large regions. It has been used in PV power station identification based on Landsat series data in recent years [15–17]. However, these studies scarcely focus on the combination of development processes and environmental effects. Therefore, this study aimed to provide a method to quickly identify and monitor the time series changes of PV power stations and to clarify the positive effect of PV power station construction on vegetation restoration and the corresponding time by normalizing vegetation index changes under different construction years.

The Landsat series of satellites has been serving global feature monitoring for about 50 years and thus has great potential for monitoring the temporal changes of PV power stations in large-scale areas. Furthermore, remote sensing cloud computing platforms such as Google Earth Engine (GEE) [18] greatly facilitate the analysis of massive amounts of data on large spatial scales over long periods of time. The most widely used methods of remote sensing image time series analysis include Breaks for Additive Seasonal and Trend (BFASST) [19,20], Detecting Breakpoints and Estimating Segments in Trend (DBEST) [21,22], Discrete wavelet transform-based trends and turning points detection (DWT-TTD) [23], and Landsat-based detection of Trends in Disturbance and Recovery (LandTrendr) [24,25]. The LandTrendr algorithm has been integrated into GEE, which is a model mainly for Landsat interannual time series to carry out time series evolution trajectory modeling and achieve turning points and feature parameter mining. It has advantages in extensive land time series monitoring.

In this study, based on the GEE platform, we used Landsat time-series images from 1990–2022 to grasp the spatial distribution and development trajectory of PV power stations in the desert region and their impact on the ecological environment. We aim to (1) construct a random forest model based on Landsat images in 2022 that combines the spectral and texture features of the images to rapidly and accurately identify the PV power stations. (2) Based on the normalized construction land index (NDBI), an interannual time series analysis of PV power station target areas was carried out using the LandTrendr algorithm to quantify the construction years and spatial and temporal trajectories of PV power station development in the study area from 1990 to 2022. (3) The normalized vegetation index (NDVI) was used as an ecological indicator variable to assess the impact of different construction years on the ecological environment.

## 2. Study Area

Our study focuses on the junction area of Inner Mongolia Autonomous Region and Ningxia Hui Autonomous Region along the banks of the Yellow River. The area is a typical ecologically fragile zone of desert oasis junction and an important area of high-quality

development in the Yellow River Basin (Figure 1). It consists of Hobq Desert, Ulan Buh Desert, Tengger Desert, and Mu Us Sands. The annual sunshine hours are more than 3300 h, and the intensity of solar radiation reached a total annual radiation of about  $6400 \text{ MJ/m}^2$ , which is an internationally recognized first-level area for solar radiation distribution.

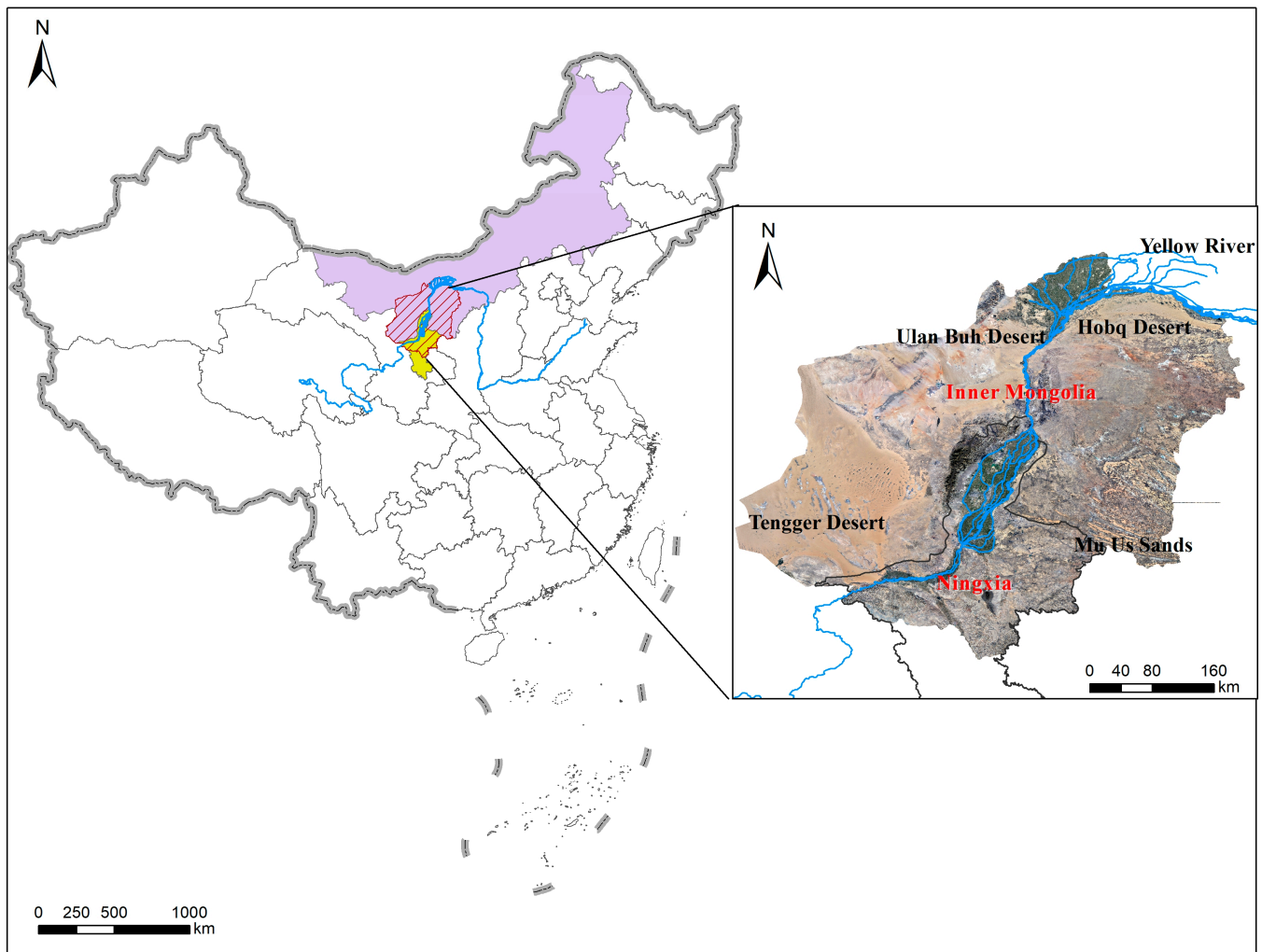


**Figure 1.** Location of the study area. The left map represents the location of the study area in China, in the border area of Ningxia and Inner Mongolia in western China. The right map is a remote photo of the study area (from Google Earth), which is surrounded by several large deserts, including Hobq Desert, Ulan Buh Desert, Tengger Desert, and Mu Us Sands.

### 3. Materials and Methods

The long-time-series remote sensing image data derived and processed using the GEE platform is the basic data of our study. Our research included three main parts, as shown in Figure 2. Firstly, we used the random forest method to extract PV power stations based on the spectral band, NDBI, and texture features of NDBI, which were calculated within sliding windows pixel by pixel. Secondly, we applied the LandTrendr algorithm to identify the turning point of the NDBI time series of PV power stations as their construction years. Thirdly, we measured the NDVI temporal change before and after the construction of PV power stations to analyze their impact on vegetation conditions.

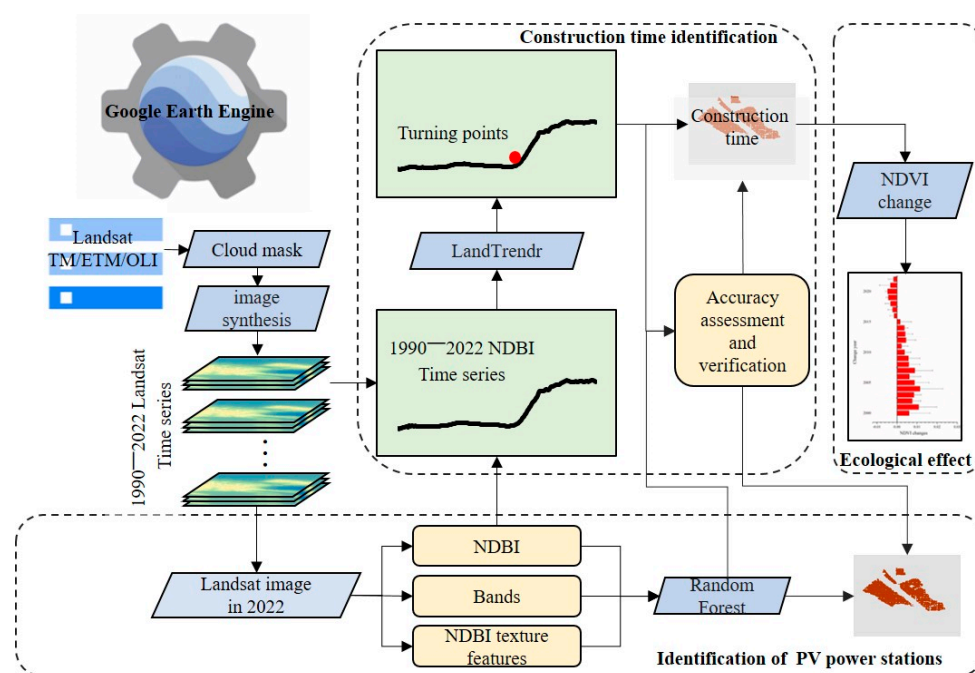


**Figure 2.** The flowchart of this method.

### 3.1. Landsat Imagery and Preprocessing

We utilized NASA's Surface Reflectance (SR) products from the Landsat satellite mission and processed the data using the GEE platform. To provide a long-term analysis of more than 30 years, we derived all available Landsat-5 TM, Landsat-7 ETM+, and Landsat-8 OLI images in the study area. A total of 10,030 images were obtained from the GEE platform, as shown in Table 1. We conducted data preprocessing to remove clouds using the Fmask band of Landsat SR data and to remove striping on Landsat 7 images (Figure 3). Additionally, a Multi-Dimensional Median method was employed for image synthesis to create a time-series image dataset.

**Table 1.** Description of parameters for different satellite sensors.

Satellite Sensor	Spatial Resolution (m)	Revisit Period (Day)	Available Date Range (Year)	Number of Images
Landsat-5	30	16	1990–2011	6271
Landsat-7	30	16	2012–2013	568
Landsat-8	30	16	2014–2022	3191

### 3.2. PV Power Station Extraction

Solar panels have special spectral properties that can be exploited to extract PV power stations from optical satellite images. Solar panels are designed to absorb visible and near-infrared light to generate electricity while reflecting most of the short-wave infrared light to prevent the panels from overheating. Therefore, solar panels have low reflectivity in the visible and near-infrared bands and high reflectivity in the short-wave infrared band. At the same time, solar panels in PV plants are regularly distributed and thus have special textures. Therefore, we extracted PV power stations by integrating spectral features and texture features using a random forest model.

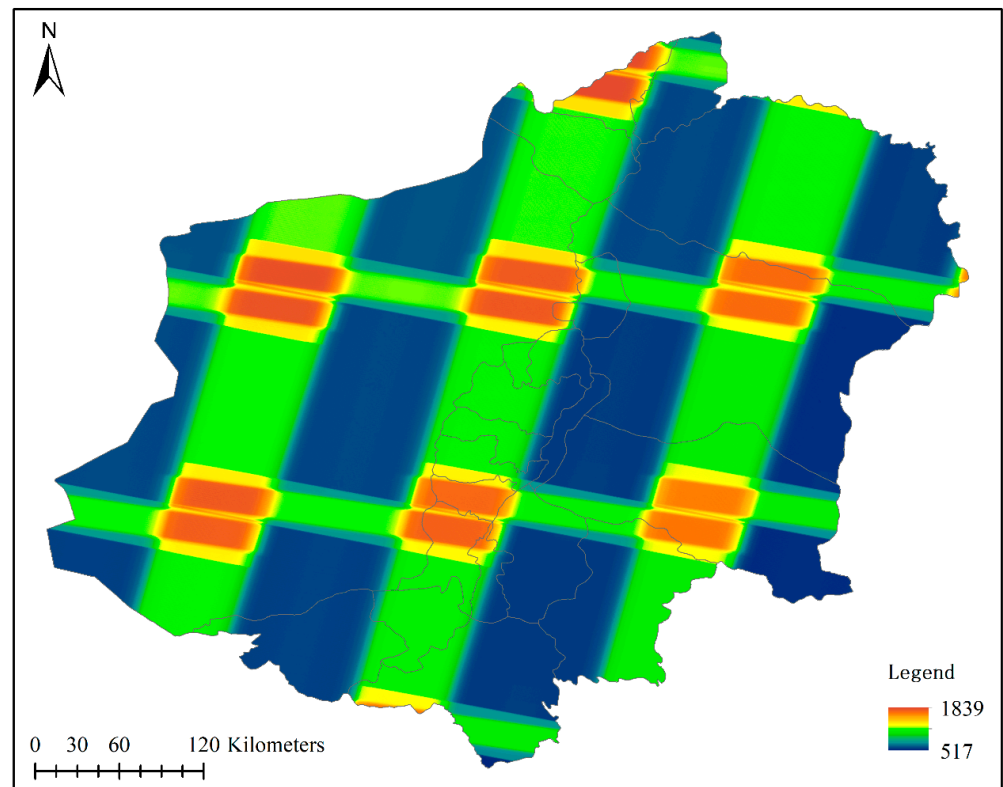


**Figure 3.** Effective observation per pixel.

### 3.2.1. Spectral Feature Selection

Seven visible bands of Landsat 8 OLI were selected as part of the spectral features. Considering the spectral characteristics of PV power stations in the short-wave infrared and near-infrared bands, we used the normalized difference built-up index (NDBI) [26] to extract PV power stations. Its expression is as follows:

$$\text{NDBI} = (\text{SWIR1} - \text{NIR}) / (\text{SWIR1} + \text{NIR}), \quad (1)$$

where SWIR1 and NIR represent the shortwave infrared band and the near-infrared band of Landsat TM/ETM+/OLI imagery, respectively.

### 3.2.2. Texture Feature Analysis

A gray-level co-occurrence matrix (GLCM) was used to describe PV texture features [27,28]. It represents the orientation, adjacent interval, and change magnitude of the target object on the image. It has been widely used in texture analysis, feature classification, and image quality evaluation [28–30]. Considering the complex shape and spectral features of PV power stations, to improve computing efficiency and reduce redundant information, we computed the texture variables from GLCM based on the NDBI. Five GLCM statistical parameters were used in the classification, which included Angular Second Moment (ASM), Correlation (CORR), Entropy (ENT), Sum Average (SAVG), and Cluster Shade (SHADE). ASM reflects the uniformity of the image gray level distribution; CORR reflects the linear dependence of the gray level of adjacent pixels; ENT indicates the degree of disorder between pixels in the image; SAVG indicates the average of the gray level and distribution of the image; and SHADE measures the skewness of the matrix and measures the concept of uniformity.

### 3.2.3. Random Forest Model

We applied a pixel-based random forest method on the GEE platform to identify the PV power stations. As a robust machine learning algorithm, the random forest method

does not need to make assumptions about the distribution of the data, and it can be used to avoid overfitting [31,32]. It has fast operation speeds and high accuracy in classification results [31–33]. It achieves better results in remote sensing image information extraction and change detection.

Based on field surveys and high-resolution Google Earth images, we selected a total of 390,833 uniformly distributed and representative samples. It included 16,667 PV power station samples and 374,167 non-PV samples (other land use types including deserts, farmland, and water bodies). We used 70% of the samples as training samples and the remaining 30% as validation samples.

To train the RF classifier, a total of 13 features were selected (Figure 4), including normalization indicators (NDBI), five texture feature bands, and seven original bands. To examine the classification accuracy, we selected test samples independently using Google Earth. We derived a total of 2000 points for PV power stations and 3500 points for non-PV, and finally calculated the accuracy evaluations using the confusion matrix.

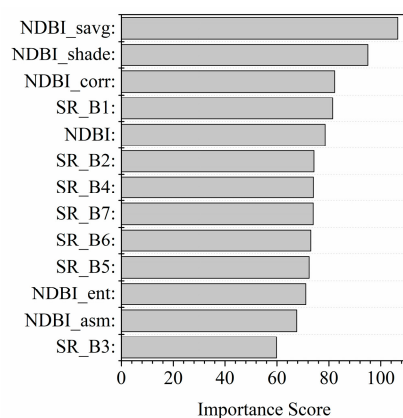


**Figure 4.** Importance score of 13 features.

### 3.3. Time Series Turning Point Detection Based on Landtrendr

LandTrendr is a set of spectral temporal segmentation algorithms that can be used for change detection for time series of medium-resolution satellite images (mainly Landsat) as well as for generating trajectory-based spectral time series data free of interannual signal noise [24,34]. To determine the construction years of PV power stations, we identified the turning points of the NDBI time series of PV land area from 1990–2022 using LandTrendr. In the LandTrendr calculation, the model input parameters were set as in Table 2.

**Table 2.** Values for control parameters used in test runs of the LandTrendr algorithms.

LandTrendr Parameter	Type	Set Values
Max Segments	Integer	6
Spike Threshold	Float	0.9
Vertex Count Overshoot	Integer	3
Prevent One Year Recovery	Boolean	true
Recovery Threshold	Float	0.25
Pval Threshold	Float	0.05
Best Model Proportion	Float	0.75
Min. Observations Needed	Integer	6

Based on the time series turning points, we determined the dominant turning points according to the characteristics of the time evolution of NDBI. To ensure the validity of the turning point, we set two criteria based on multiple experiments: the change magnitude should be larger than 0.05, while the duration (period from start to end) should be shorter than 4 years (Figure 5).

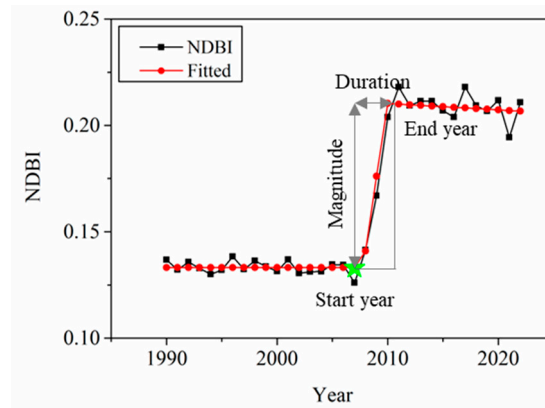


**Figure 5.** Temporal trend-turning points.

To verify the accuracy of PV power station construction year identification, 100 points were randomly selected in the PV area. We then determined the emergence time of PV power stations at the points according to Google Earth historical images and used them as the measured construction year. Based on the paired reference and estimated change year within the points, we adopt four accuracy metrics, including mean error ( $ME$ ), mean absolute error ( $MAE$ ), root mean square error ( $RMSE$ ), and  $R^2$ , to assess the accuracy.

$$ME = \frac{\sum_{i=1}^n (p_i - r_i)}{n} \quad (2)$$

$$MAE = \frac{\sum_{i=1}^n |p_i - r_i|}{n} \quad (3)$$

$$RMSE = \sqrt{\frac{\sum_{i=1}^n (p_i - r_i)^2}{n}} \quad (4)$$

$$R^2 = 1 - \frac{\sum_{i=1}^n (p_i - r_i)^2}{\sum_{i=1}^n (p_i - \bar{r})^2} \quad (5)$$

where  $p_i$  and  $r_i$  are estimated and reference change years at  $i$  points,  $n$  is the sample size, and  $\bar{r}$  is the mean of the reference change years of all points.

### 3.4. Assessment of the Ecological Impact of PV Power Station Construction

We hypothesize that there has been continuous variability in the ecological status since the PV power stations were constructed. Therefore, we compared the normalized difference vegetation index ( $NDVI$ ) changes of PV power stations constructed in different years [8]. First, we calculated the mean  $NDVI$  from 1990 to the construction year as the average vegetation condition before the construction. Secondly, we calculated the  $NDVI$  value in 2022 as the current vegetation condition. Finally, we calculated the difference between the precedent mean  $NDVI$  and the current  $NDVI$  to assess the ecological impact of PV power stations.

$$NDVI_{change} = NDVI_{2022} - NDVI_{pre} \quad (6)$$

where  $NDVI_{change}$  is the  $NDVI$  change,  $NDVI_{2022}$  is the mean  $NDVI$  in 2022,  $NDVI_{pre}$  is the mean  $NDVI$  from 1990 to the construction year, which is the pre-construction average  $NDVI$ .

## 4. Results

### 4.1. Mapping of PV Power Stations

#### 4.1.1. Accuracy Assessment and Verification

We identified the PV power stations by combining spectral and texture information using a random forest model. The results of 30% of validation samples showed an overall

accuracy higher than 99%. The results of the validation sample accuracy evaluation show that (Table 3), the overall accuracy of the classification is 96.65% and the Kappa coefficient is 0.92. Among all 2000 validation sample points of PV power stations, 167 sample points were misclassified as other sites; among all 3500 validation sample points of non-PV power stations, 17 other sites were misclassified as PV sites. As shown in Figure 6, the boundaries of the extracted target area are generally good. Overall, the accuracy assessments demonstrated that the classification results could meet the criteria for spatial analysis, and the impact of classification errors on the analysis results in this study is relatively small.

**Table 3.** Validation of the accuracy of the classification result.

	Ground Truth (Pixels)		Producer Accuracy	User Accuracy
	PV Power Stations	Others		
PV power stations	1833	17	0.9165	0.9908
Others	167	3483	0.9951	0.9542
Overall accuracy	0.9665			
Kappa	0.9264			

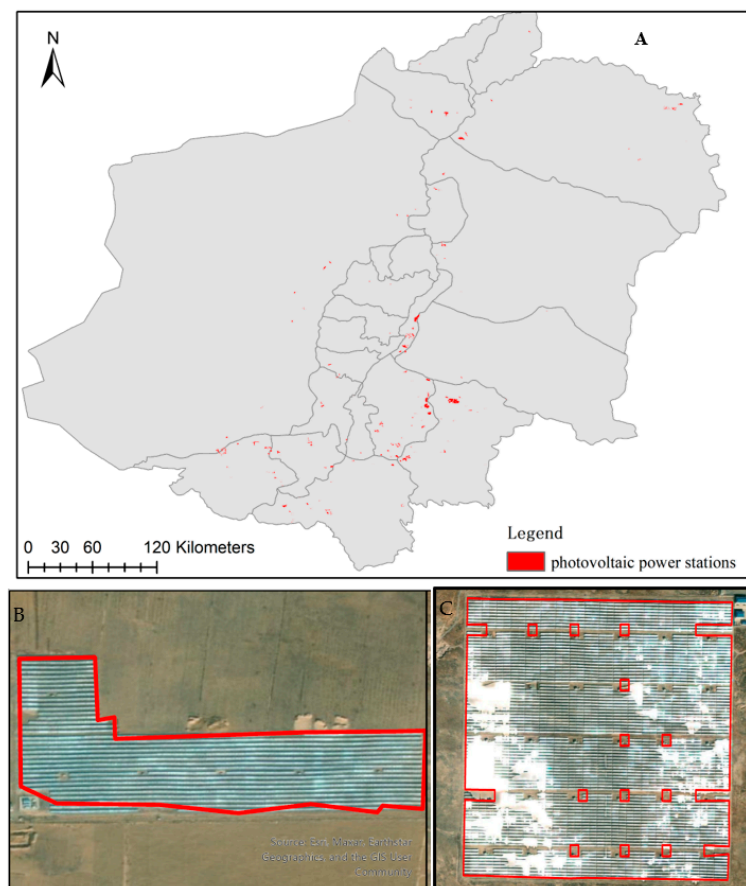


**Figure 6.** Validation of the accuracy of the classification result. (A) Spatial distribution of PV power stations; (B,C) the boundary of identified PV power station.

#### 4.1.2. Distribution of PV Power Stations

Regarding the construction area, the total area of PV power stations reached 115.61 km<sup>2</sup> (Figure 7A,B). Ningxia has the largest area of PV power stations. They are mostly located in the Mu Us Sands and Tengger Desert, involving the administrative districts of Lingwu City, Yanchi County, and Zhongwei City. In terms of the type of land where PV power

stations were constructed, the land types are mainly sand and bare land. The extraction application demonstration of PV power stations in this region provides data support for the spatial monitoring and management of PV power stations and provides a reference for future planning and design and rational utilization of resources.

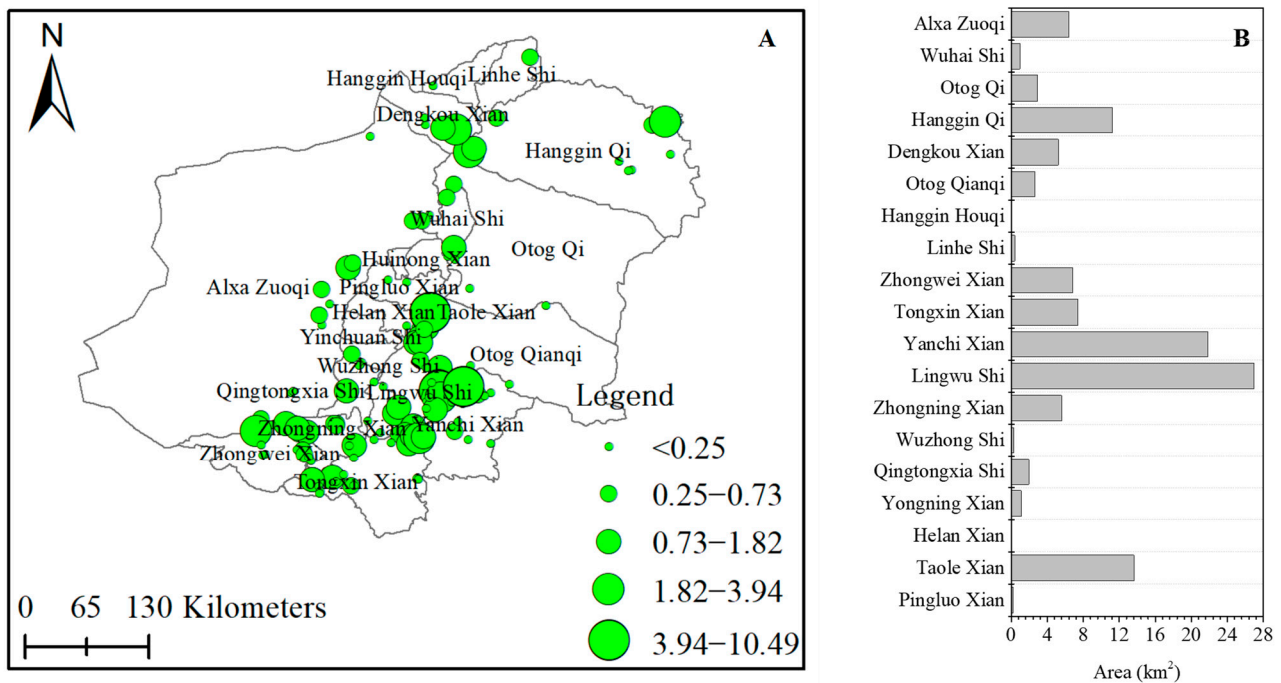


**Figure 7.** Spatial distribution of PV power stations. (A) Spatial distribution of PV power stations displayed with their area; (B) PV power station area in each county of the study area.

#### 4.2. Construction and Identification of PV Power Stations

We successfully employed the LandTrendr algorithm to detect the turning point of the NDBI time series for identifying the construction year of the PV power station (Figure 8). By selecting 100 sample points and conducting turning point time verification on Google Earth, the study collected 69 sets of valid data for accuracy verification (Figure 9A,B). The results revealed that the method achieved high accuracy, with MAE and ME of PV power station age both less than 0.1 and RMSE less than 0.5 (Figure 9C). While there were some age prediction errors of individual image pixels that were greater than 4 years, the overall age prediction difference was within 3 years, indicating that the method can extract the age of PV power stations relatively accurately.

Based on the LandTrendr algorithm, the 30-year PV power station dynamics from 1990–2022 were monitored, and the PV power station construction years from 1990–2022 were identified (Figure 10B). The trend of PV power station construction is growing, with an average annual change of 3.65 km<sup>2</sup> in the total area of PV power station construction from 1990 to 2022. The annual construction area of PV power stations was very low before 2010 (<2 km<sup>2</sup>), and the stations were mainly built in the central part of the study area (Figure 10A,B). However, an obvious spike in newly built PV power stations appeared after 2010. The annual construction area reached a peak of 14.52 km<sup>2</sup> in 2016, accounting for 47.19% of the total construction area from 2010 to 2016. The PV power stations constructed during this period were distributed from the central region to all regions. After 2016, the number of PV power stations constructed per year fluctuated and decreased but remained at a high level. The PV power stations constructed after 2016 were mainly located in the southern and northern regions of the study area (Figure 10A,B).

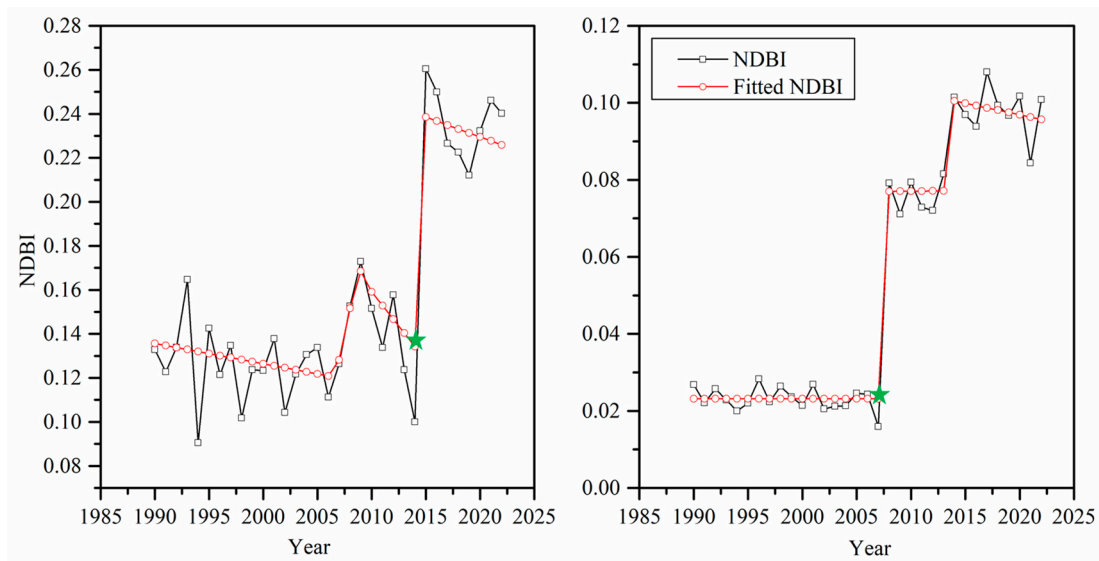


Figure 8. NDBI time series turning point detection by the LandTrendr.

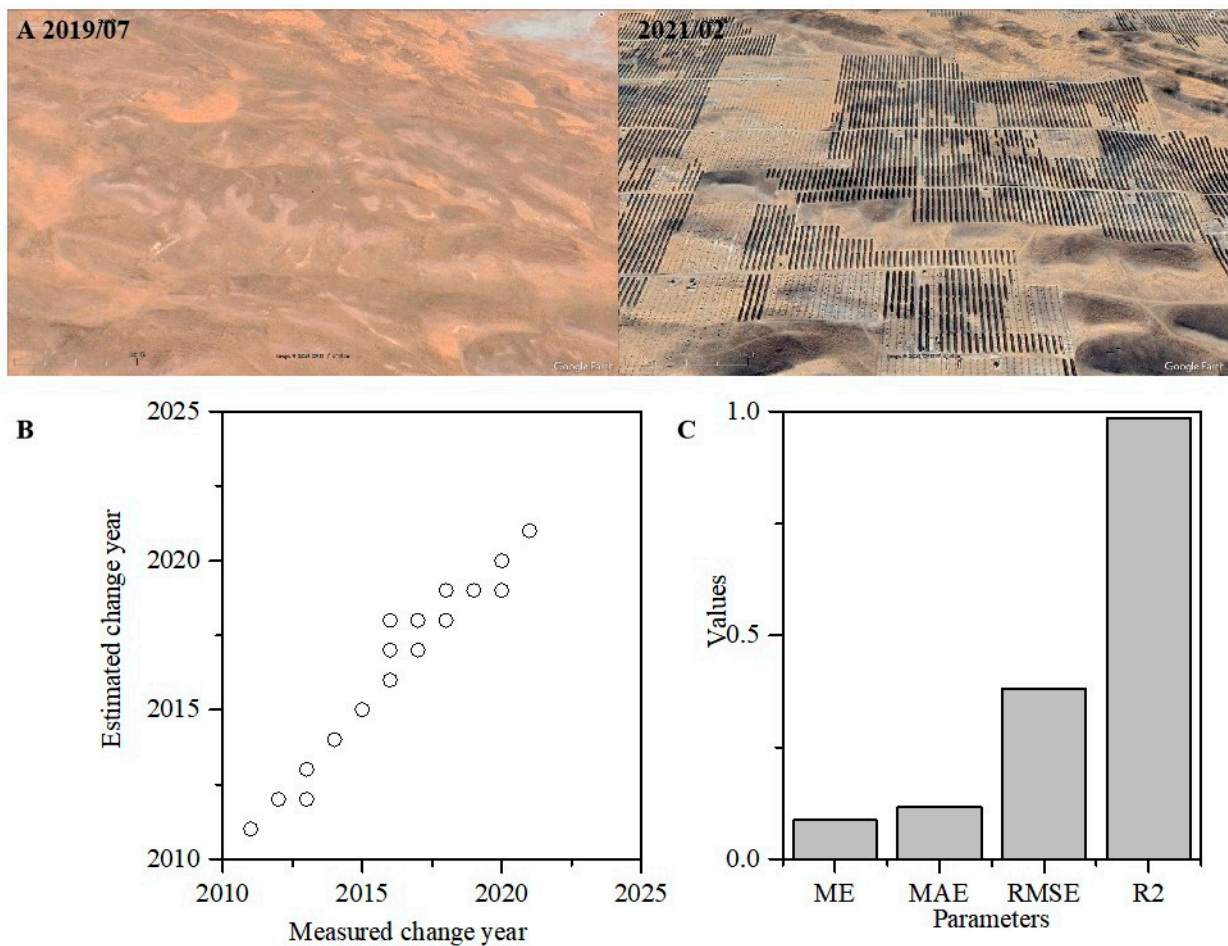
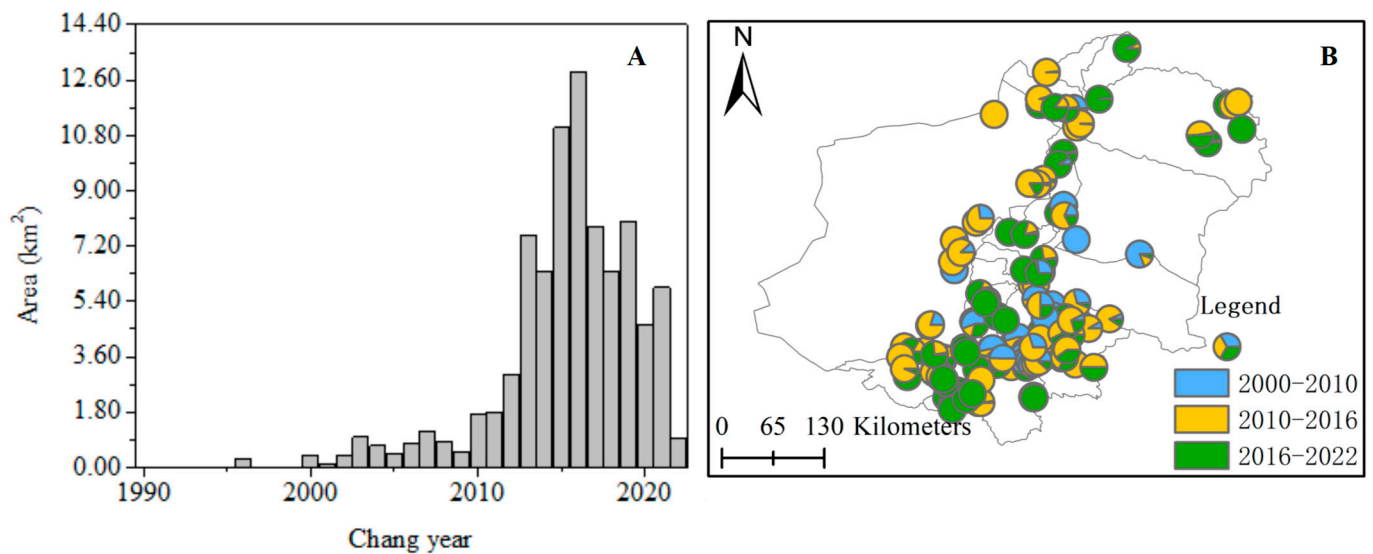


Figure 9. Validation of turning point detection results. (A) An example of the construction year of the PV power station; (B) valid data collected; (C) The values of MAE, ME, RMSE and R<sup>2</sup>.



**Figure 10.** The construction years of PV power stations. (A) The area of new construction each year; (B) the spatial distribution of PV power stations constructed in different years.

#### 4.3. Vegetation Condition Change in PV Power Stations Constructed in Different Years

We used NDVI as an ecological indicator to assess the vegetation condition of PV power stations before and after they were constructed and compared the NDVI changes of PV power stations constructed in different years. The results (Figure 11A) showed a negative NDVI change for PV power stations constructed after 2016. It implied that during the initial period of construction, current vegetation was often damaged. Meanwhile, the NDVI change for PV power stations constructed in 2020 reached a low point. The NDVI change in the former period (2016–2022) is related to the gradual recovery of vegetation after the completion of PV power stations, implying that vegetation can reach the average level before construction in a 5-year cycle, and the NDVI change in the latter period (2020–2022) is related to the construction cycle of PV power stations, which can also be consistent with the perception that vegetation is occupied during the project advancement. On the contrary, the NDVI changes for PV power stations constructed before 2016 were all positive. It implies that when the PV power stations were built for more than 6 years, the NDVI exceeded the pre-construction average, and the increase in NDVI has also been expanding with the construction time.

We further chose two PV power stations to analyze their NDVI changes from 1990 to 2020 (Figure 11B,C). For both stations, the NDVI showed fluctuations before their construction, a short-term decline about 2 years after construction, followed by a rapid rise reaching the pre-construction level, and a continuous rise.

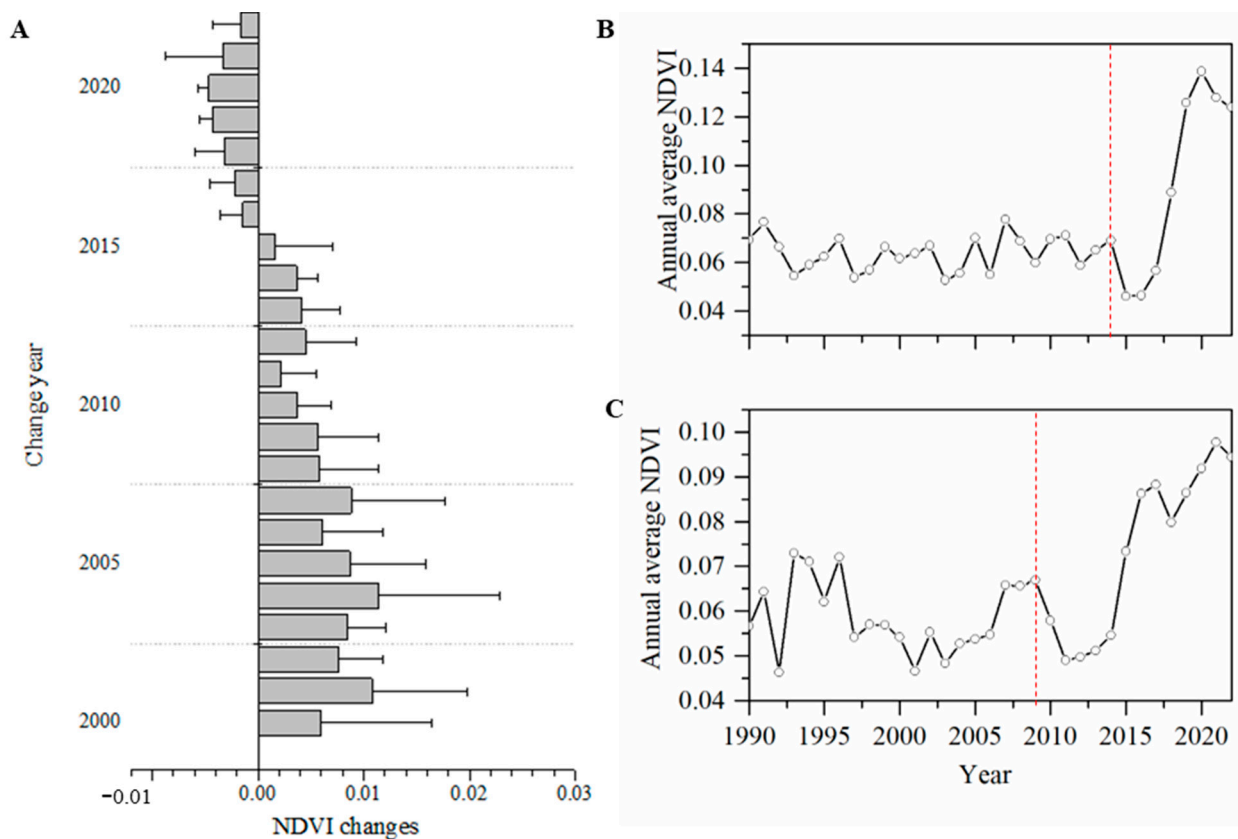


**Figure 11.** The NDVI change of PV power stations constructed in different years. (A) mean value and error bar of NDVI change; (B,C) annual average NDVI time series of two PV power stations, constructed in 2013 and 2009 (the red dotted lines represent their construction year).

## 5. Discussion

### 5.1. Comparison between the RF Model and the Deep Learning Model

We compare the accuracy of the RF model with the deep learning model in identifying PV power stations. We used ArcGIS Pro 2.8 to conduct sample labeling through manual visualization and generated samples with a size of 128\*128 pixels. We then enlarged the sample using two data augmentation methods, including mirrored transform approaches (i.e., left and right; up and down) and rotated transform approaches (i.e., 0°, 90°, 180°, and 270°) [32]. We finally obtained 1592 valid samples. With 20% of these samples as validation samples, we used the U-net model to train the model and conducted the prediction in ArcGIS Pro 2.8. Epoch, learning rates, and mini-batch parameters were respectively set to 20, 0.01, and 2.

The loss curve of the deep learning model showed a decreasing trend. Especially when the epoch is greater than 8, the loss curves of training samples and validation samples were around 0.2 and 0.9, and the accuracy reached 98% (Figure 12A). Regarding the accuracy of identification, precision, recall, and the F1 index, they nearly reach 1 (Figure 12B,C). It indicates that the deep learning model achieved higher accuracy than the RF model. However, we used the RF model to integrate spectral bands, spectral indices, and texture features. It balanced the classification accuracy and time efficiency compared with the time-consuming and labor-intensive sample labeling in the deep learning model. Therefore, the RF model is suitable for classification based on massive medium-spatial-resolution images.

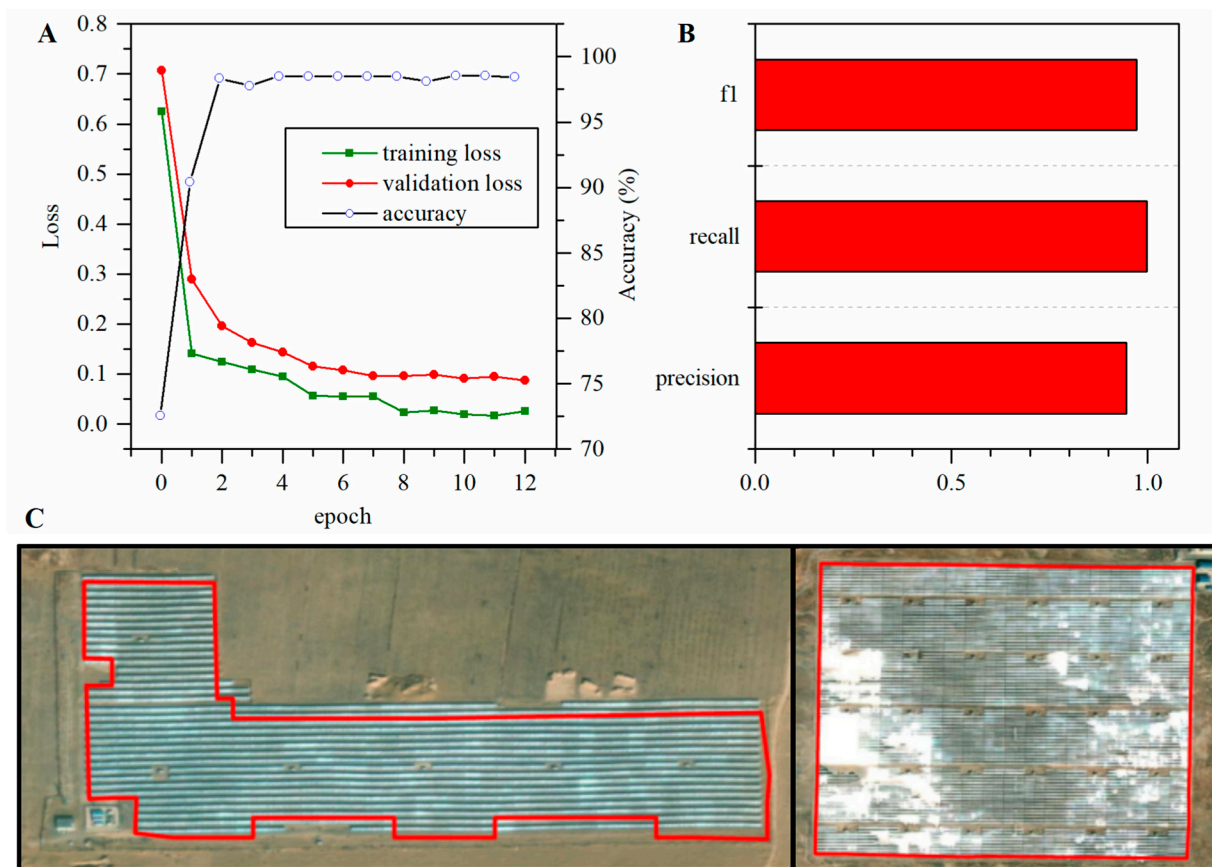


**Figure 12.** Comparisons with deep learning. (A) Loss and accuracy change with epoch; (B) accuracy index, including f1 score, recall, and precision; (C) the boundary of identified PV power station.

### 5.2. Characterizing the Development of PV Power Stations

Based on the long-time series of medium-resolution satellite images, we used the Random Forest model and LandTrendr algorithm to identify PV power stations and their construction years. This method helps to quickly map PV power stations and their development trajectory because of its high accuracy and stable algorithm. This method is expected to be extended to other regions in western China where PV power stations are built on a large scale. However, due to the high heterogeneity of the regional landscape and the extremely vulnerable surface conditions in arid areas, there are certain errors in the identification of PV sites. In the future, integrating high-spatial-resolution images and advanced methods such as deep learning models may help improve the accuracy of PV power station classification. Furthermore, there are also some errors in turning points detected by the Landtrendr model, especially the detection of some turning points earlier than 2008, which is not consistent with reality. Therefore, the model needs to be improved or restricted through practical knowledge to improve the accuracy of time series turning point detection.

Energy policies are the main factor driving the rapid development of PV power stations in China [35]. Since 2004, PV production in China has experienced tremendous growth due to the dramatic increase in demand for PV in European countries. To promote the domestic deployment of PV, China launched a national solar subsidy program in 2009 [36,37]. In addition, China has developed a series of policy incentives, including the Photovoltaic Poverty Alleviation Program [38,39], which has led to a rapid increase in PV construction in China. The fact that the construction of PV power stations grew rapidly after 2010 is consistent with the trend of national policies.

### 5.3. Ecological Effects of PV Power Station Construction

Our research found that the vegetation cover level was restored to the pre-construction average level after 5–6 years of PV power station construction and continues to improve over time. Such a positive impact on vegetation conditions may result from the efforts of PV power station builders, operators, and the government in implementing the “photovoltaic control” model. The model balances PV power generation and desert treatment to realize both economic and ecological benefits. According to the model, PV power generation is used as the power source. At the same time, drip irrigation facilities are installed. Plants, including small shrubs and forage, are planted under the photovoltaic panels. Around the periphery of the power station, grass-square sand barriers and sand fixation forestry form a protective forest system. It solves not only the power supply problem of desertification control but also the bottleneck constraint of difficult new energy transmission. According to the estimation, constructing a 1 million KW photovoltaic sand control project in a desert area would save about 440,000 tons of standard coal per year. The area of wind and sand control reaches 40 million m<sup>2</sup>, which is equivalent to planting 640,000 trees [40]. In addition, studies have proved that PV power station construction may reduce the evaporation of the ground and therefore have a positive effect on vegetation recovery.

Therefore, on the one hand, constructing desert PV power stations helps to realize the win-win of clean energy and promotes the transformation of the energy structure. On the other hand, it plays a positive role in restoring vegetation, preventing wind, fixing sand, and protecting the ecological environment. Western China is a vast area with sufficient light intensity. Considering the advantages of PV construction in terms of ecological restoration and economic outcome, the construction of more PV stations in the northwest can be carried out with systematic consideration. Specifically, solar radiation, terrain conditions, meteorological conditions, land resources, and transportation should be taken into account to make reasonable spatial layout and management decisions for PV power stations. Under the background of “carbon peaking and carbon neutrality”, it is of great significance for the scientific development of new energy in China and plays an important role in the early realization of the dual carbon goals.

Admittedly, this study selected only NDVI as the indicator characterizing the ecological condition to assess the ecological effect of PV power stations. In future research, it is necessary to carry out field observation at large-scale PV power stations in desert areas to assess their effect on local microclimate and biodiversity. Furthermore, we believe that future studies can incorporate vegetation recovery trends of PV power stations under global climate change and anthropogenic activities, with a view to providing a basis for us to carry out ecological and environmental early warning and management.

## 6. Conclusions

This study introduces a new comprehensive method for mapping PV power stations in desert oasis regions of China. The method integrates texture features and spectral features using a random forest algorithm in GEE. It can be applied to the analysis of large-scale PV power stations. The method has a low computational cost and introduces time series analysis based on medium-resolution images that are freely available. It contributes to studies on the spatial and temporal dynamics of PV power development. The results showed a total area of 109.53 km<sup>2</sup> of PV power station construction from 1990–2022. The fastest growth was found from 2010 to 2016, mainly distributed in the Mu Us Desert and Tengger Desert in Ningxia. The rapid expansion of PV power stations in the past few years was driven mainly by national renewable energy policies. The time series of NDVI in PV power stations showed a short-term decline after their construction and a subsequent continuous rise that even exceeded the pre-construction average level. It may imply a positive long-term impact of PV power stations on vegetation conditions. This finding is of great importance for renewable energy planning, management, and sustainable development.

**Author Contributions:** Conceptualization, S.M., P.Z. and J.L.; methodology, S.M. and P.Z.; software, S.M.; validation, S.M.; data curation, S.M., J.Z., Y.L. and Y.Z.; writing—original draft preparation, S.M.; writing—review and editing, J.L., X.T. and P.Z.; visualization, S.M.; supervision, P.Z.; project administration, J.L.; funding acquisition, J.L. All authors have read and agreed to the published version of the manuscript.

**Funding:** This research was funded by the National Key Research and Development Program of China (No. 2016YFB0501505).

**Data Availability Statement:** The PV mapping code: <https://code.earthengine.google.com/65bee1fd5b94b0ee1fe66ee86686a1d1> (accessed on 4 June 2023). Change year code: <https://code.earthengine.google.com/3e3cd41dad4f168cc0abd3975cf83d21> (accessed on 4 June 2023).

**Acknowledgments:** All figures in this paper were generated in ArcMap 10.5 and Origin 2021. The authors would like to thank the editors and anonymous reviewers for their constructive comments and suggestions.

**Conflicts of Interest:** The authors declare no conflict of interest.

## References

1. Tao, S.; Rogan, J.; Ye, S.; Geron, N. Mapping photovoltaic power stations and assessing their environmental impacts from multi-sensor datasets in Massachusetts, United States. *Remote Sens. Appl. Soc. Environ.* **2023**, *30*, 100937. [CrossRef]
2. Shahsavari, A.; Akbari, M. Potential of solar energy in developing countries for reducing energy-related emissions. *Renew. Sustain. Energy Rev.* **2018**, *90*, 275–291. [CrossRef]
3. Bahadori, A.; Nwaoha, C. A review on solar energy utilisation in Australia. *Renew. Sustain. Energy Rev.* **2013**, *18*, 1–5. [CrossRef]
4. Panwar, N.L.; Kaushik, S.C.; Kothari, S. Role of renewable energy sources in environmental protection: A review. *Renew. Sustain. Energy Rev.* **2011**, *15*, 1513–1524. [CrossRef]
5. Wang, Y.; Gao, M.; Wang, J.; Wang, S.; Tan, Z. Measurement and key influencing factors of the economic benefits for China's photovoltaic power generation: A LCOE-based hybrid model. *Renew. Energy* **2021**, *169*, 935–952. [CrossRef]
6. Xu, M. Texture Is Important in Improving the Accuracy of Mapping Photovoltaic Power Plants: A Case Study of Ningxia Autonomous Region, China. *Remote Sens.* **2021**, *13*, 3909. [CrossRef]
7. Jiang, W.; Tian, B.; Duan, Y.; Chen, C.; Hu, Y. Rapid mapping and spatial analysis on the distribution of photovoltaic power stations with Sentinel-1&2 images in Chinese coastal provinces. *Int. J. Appl. Earth Obs. Geoinf.* **2023**, *118*, 103280. [CrossRef]
8. Xia, Z.; Li, Y.; Zhang, W.; Chen, R.; Guo, S.; Zhang, P.; Du, P. Solar photovoltaic program helps turn deserts green in China: Evidence from satellite monitoring. *J. Environ. Manag.* **2022**, *324*, 116338. [CrossRef] [PubMed]
9. Hu, Y.; Tian, B.; Yuan, L.; Li, X.; Sun, C. Mapping coastal salt marshes in China using time series of Sentinel-1 SAR. *ISPRS J. Photogramm. Remote Sens.* **2021**, *173*, 122–134. [CrossRef]
10. Bradbury, K.; Saboo, R.; Johnson, T.L.; Malof, J.M.; Devarajan, A.; Zhang, W.; Collins, L.M.; Newell, R.G. Distributed solar photovoltaic array location and extent dataset for remote sensing object identification. *Sci. Data* **2016**, *3*, 160106. [CrossRef] [PubMed]
11. Jie, Y.; Liu, A.; Huang, Q.; Chen, J.; Meng, Y.; Deng, Y.; Yu, Z. Photovoltaic power station identification using refined encoder-decoder network with channel attention and chained residual dilated convolutions. *J. Appl. Remote Sens.* **2020**, *14*, 6506. [CrossRef]
12. Jie, Y.; Ji, X.; Yue, A.; Chen, J.; Zhang, Y. Combined Multi-Layer Feature Fusion and Edge Detection Method for Distributed Photovoltaic Power Station Identification. *Energies* **2020**, *13*, 6742. [CrossRef]
13. Lima, M.; Fernandez-Ramirez, L.M.; Carvalho, P.; Batista, J.G.; Freitas, D.M. A comparison between Deep Learning and Support Vector Regression Techniques applied to solar forecast in Spain. *J. Sol. Energy Eng.* **2022**, *144*, 010802. [CrossRef]
14. Zhang, X.; Han, L.; Han, L.; Zhu, L. How Well Do Deep Learning-Based Methods for Land Cover Classification and Object Detection Perform on High Resolution Remote Sensing Imagery? *Remote Sens.* **2020**, *12*, 417. [CrossRef]
15. Zhu, R.; Guo, D.; Wong, M.S.; Qian, Z.; Chen, M.; Yang, B.; Chen, B.; Zhang, H.; You, L.; Heo, J.; et al. Deep solar PV refiner: A detail-oriented deep learning network for refined segmentation of photovoltaic areas from satellite imagery. *Int. J. Appl. Earth Obs. Geoinf.* **2023**, *116*, 103134. [CrossRef]
16. Xia, Z.; Li, Y.; Chen, R.; Sengupta, D.; Guo, X.; Xiong, B.; Niu, Y. Mapping the rapid development of photovoltaic power stations in northwestern China using remote sensing. *Energy Rep.* **2022**, *8*, 4117–4127. [CrossRef]
17. Xia, Z.; Li, Y.; Guo, X.; Chen, R. High-resolution mapping of water photovoltaic development in China through satellite imagery. *Int. J. Appl. Earth Obs. Geoinf.* **2022**, *107*, 102707. [CrossRef]
18. Gorelick, N.; Hancher, M.; Dixon, M.; Ilyushchenko, S.; Thau, D.; Moore, R. Google Earth Engine: Planetary-scale geospatial analysis for everyone. *Remote Sens. Environ.* **2017**, *202*, 18–27. [CrossRef]
19. Xu, L.; Herold, M.; Tsensbazar, N.-E.; Masiliūnas, D.; Li, L.; Lesiv, M.; Fritz, S.; Verbesselt, J. Time series analysis for global land cover change monitoring: A comparison across sensors. *Remote Sens. Environ.* **2022**, *271*, 112905. [CrossRef]

20. Verbesselt, J.; Hyndman, R.; Newnham, G.; Culvenor, D. Detecting trend and seasonal changes in satellite image time series. *Remote Sens. Environ.* **2010**, *114*, 106–115. [\[CrossRef\]](#)
21. Jamali, S.; Jönsson, P.; Eklundh, L.; Ardö, J.; Seaquist, J. Detecting changes in vegetation trends using time series segmentation. *Remote Sens. Environ.* **2015**, *156*, 182–195. [\[CrossRef\]](#)
22. Kazemzadeh, M.; Noori, Z.; Alipour, H.; Jamali, S.; Seyednasrollah, B. Natural and anthropogenic forcings lead to contrasting vegetation response in long-term vs. short-term timeframes. *J. Environ. Manag.* **2021**, *286*, 112249. [\[CrossRef\]](#) [\[PubMed\]](#)
23. Sun, Q.; Zhang, P.; Jiao, X.; Han, W.; Sun, Y.; Sun, D. Identifying and understanding alternative states of dryland landscape: A hierarchical analysis of time series of fractional vegetation-soil nexuses in China's Hexi Corridor. *Landsc. Urban Plan.* **2021**, *215*, 104225. [\[CrossRef\]](#)
24. Kennedy, R.E.; Yang, Z.; Cohen, W.B. Detecting trends in forest disturbance and recovery using yearly Landsat time series: 1. LandTrendr—Temporal segmentation algorithms. *Remote Sens. Environ.* **2010**, *114*, 2897–2910. [\[CrossRef\]](#)
25. Kennedy, R.E.; Yang, Z.; Gorelick, N.; Braaten, J.; Cavalcante, L.; Cohen, W.B.; Healey, S. Implementation of the LandTrendr Algorithm on Google Earth Engine. *Remote Sens.* **2018**, *10*, 691. [\[CrossRef\]](#)
26. Zha, Y.; Gao, J.; Ni, S. Use of normalized difference built-up index in automatically mapping urban areas from TM imagery. *Int. J. Remote Sens.* **2003**, *24*, 583–594. [\[CrossRef\]](#)
27. Haralick, R.M.; Shanmugam, K.; Dinstein, I. Textural Features for Image Classification. *Stud. Media Commun.* **1973**, *SMC-3*, 610–621. [\[CrossRef\]](#)
28. Du, P.; Samat, A.; Waske, B.; Liu, S.; Li, Z. Random Forest and Rotation Forest for fully polarized SAR image classification using polarimetric and spatial features. *ISPRS J. Photogramm. Remote Sens.* **2015**, *105*, 38–53. [\[CrossRef\]](#)
29. Tassi, A.; Vizzari, M. Object-Oriented LULC Classification in Google Earth Engine Combining SNIC, GLCM, and Machine Learning Algorithms. *Remote Sens.* **2020**, *12*, 3776. [\[CrossRef\]](#)
30. Rodriguez-Galiano, V.F.; Chica-Olmo, M.; Abarca-Hernandez, F.; Atkinson, P.M.; Jeganathan, C. Random Forest classification of Mediterranean land cover using multi-seasonal imagery and multi-seasonal texture. *Remote Sens. Environ.* **2012**, *121*, 93–107. [\[CrossRef\]](#)
31. Belgiu, M.; Drăguț, L. Random forest in remote sensing: A review of applications and future directions. *ISPRS J. Photogramm. Remote Sens.* **2016**, *114*, 24–31. [\[CrossRef\]](#)
32. Gislason, P.O.; Benediktsson, J.A.; Sveinsson, J.R. Random Forests for land cover classification. *Pattern Recognit. Lett.* **2006**, *27*, 294–300. [\[CrossRef\]](#)
33. Phalke, A.R.; Özdoğan, M.; Thenkabail, P.S.; Erickson, T.; Gorelick, N.; Yadav, K.; Congalton, R.G. Mapping croplands of Europe, Middle East, Russia, and Central Asia using Landsat, Random Forest, and Google Earth Engine. *ISPRS J. Photogramm. Remote Sens.* **2020**, *167*, 104–122. [\[CrossRef\]](#)
34. Matas-Granados, L.; Pizarro, M.; Cayuela, L.; Domingo, D.; Gómez, D.; García, M.B. Long-term monitoring of NDVI changes by remote sensing to assess the vulnerability of threatened plants. *Biol. Conserv.* **2022**, *265*, 109428. [\[CrossRef\]](#)
35. Yang, Y.; Campana, P.E.; Yan, J. Potential of unsubsidized distributed solar PV to replace coal-fired power plants, and profits classification in Chinese cities. *Renew. Sustain. Energy Rev.* **2020**, *131*, 109967. [\[CrossRef\]](#)
36. Zhang, H.; Zhang, X.; Yuan, J. Transition of China's power sector consistent with Paris Agreement into 2050: Pathways and challenges. *Renew. Sustain. Energy Rev.* **2020**, *132*, 110102. [\[CrossRef\]](#)
37. Xiong, Y.; Yang, X. Government subsidies for the Chinese photovoltaic industry. *Energy Policy* **2016**, *99*, 111–119. [\[CrossRef\]](#)
38. Wang, Z.; Huang, F.; Liu, J.; Shuai, J.; Shuai, C. Does solar PV bring a sustainable future to the poor?—An empirical study of anti-poverty policy effects on environmental sustainability in rural China. *Energy Policy* **2020**, *145*, 111723. [\[CrossRef\]](#)
39. Li, J.; Wang, Z.; Cheng, X.; Shuai, J.; Shuai, C.; Liu, J. Has solar PV achieved the national poverty alleviation goals? Empirical evidence from the performances of 52 villages in rural China. *Energy* **2020**, *201*, 117631. [\[CrossRef\]](#)
40. Chen, X.-J.; Jia, L.-Q.; Jia, T.; Hao, Z.-G. An carbon neutrality industrial chain of “desert-photovoltaic power generation-ecological agriculture”: Practice from the Ulan Buh Desert, Dengkou, Inner Mongolia. *China Geol.* **2022**, *5*, 549–552. [\[CrossRef\]](#)

**Disclaimer/Publisher's Note:** The statements, opinions and data contained in all publications are solely those of the individual author(s) and contributor(s) and not of MDPI and/or the editor(s). MDPI and/or the editor(s) disclaim responsibility for any injury to people or property resulting from any ideas, methods, instructions or products referred to in the content.